Supporting Information

Triangular Triplatinum Complex with Four Bridging Si-ligands. Dynamic Behavior of the Molecule and Catalysis

Makoto Tanabe, Megumi Kamono, Kimiya Tanaka, and Kohtaro Osakada*

Laboratory for Chemistry and Life Science, Institute of Innovative Research,

Tokyo Institute of Technology

4259-R1-3 Nagatsuta, Midori-ku, Yokohama 226-8503, Japan

E-mail: kosakada@res.titech.ac.jp

Table of contents

Estimation of Equilibrium Constants between 1 and 2. Equilibrium constants of the following equation were determined by comparing of the ^{1}H NMR signals assigned to *ortho* hydrogens of **1a-c**, diarylsilanes, and **2a-c** at 293, 303, 313, and 323 K.

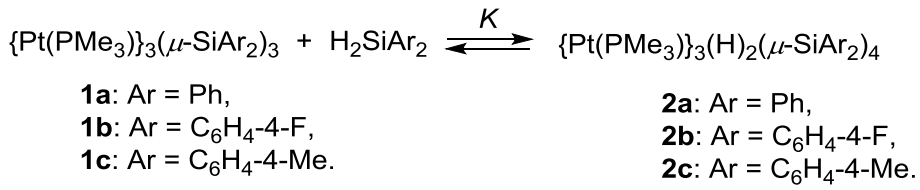

Table S1. Equilibrium Constants and Thermodynamic Parameters of **1a-c** and **2a-c**

	K_{293} [mol^{-1}]	K_{303} [mol^{-1}]	K_{313} [mol^{-1}]	K_{323} [mol^{-1}]	$\Delta G°$ [kJ mol^{-1}]	$\Delta H°$ [kJ mol^{-1}]	ΔS [J mol^{-1}K^{-1}]
1a	36.6	16.70	9.14	5.01	-7.96	-51.7	-146.9
1b	77.1	38.84	24.2	12.0	-9.95	-47.5	-126.1
1c	16.6	6.58	4.00	2.57	-5.85	-48.2	-142.1

DFT Calculations. All calculations were performed with the Gaussian 09 program package (revision E.01).[1)] The structures of **2a** and [{Pt(PMe$_3$)}$_2$(μ-η^2-HSiPh$_2$)$_2$] were optimized by density functional theory (DFT) using the MPWB95 functional in conjunction with 6-31G(d,p) basis set (for H, C, P, and Si) and SDD basis set (for Pt). The density fitting procedure was used in conjunction with W06 auxiliary basis set that implemented in Gaussian 09. All optimized structures were verified to be local minima by hessian calculation. Cartesian coordinates of **2a** and [{Pt(PMe$_3$)}$_2$(μ-η^2-HSiPh$_2$)$_2$] are provided as a "xyz" file format.

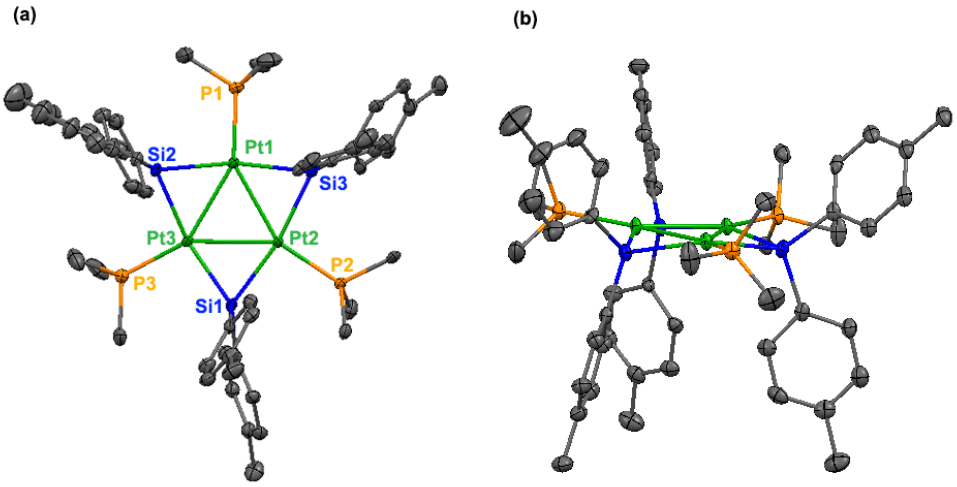

Figure S1. ORTEP drawings of (a) **1c** and (b) the side view (50% probability).

Table S2. Selected Bond Distances [Å] and Angles [deg] of Complexes **1a-c**[a]

	1a[b] (Ar = C_6H_5)	**1b**[c] (Ar = C_6H_4-4-F)	**1c** (Ar = C_6H_4-4-Me)
Pt–Pt	2.697(1)-2.716(1) (2.709(1))	2.7259(7)-2.7514(7) (2.737(7))	2.7018(8)-2.7093(5) (2.706(8))
Pt–Si	2.337(5)-2.364(5) (2.350(5))	2.342(3)-2.373(2) (2.350(3))	2.338(2)-2.375(2) (2.354(2))
Pt–P	2.226(5)-2.247(4) (2.239(5))	2.259(3)-2.265(2) (2.261(3))	2.2246(2)-2.237(2) (2.240(2))
Pt–Pt–Pt	59.57(3)-60.17(3) (60.0(3))	59.60(2)-60.52(2) (60.00(2))	59.844(1)-60.122(2) (60.00(2))
Pt–Si–Pt	70.2(1)-70.5(1) (70.4(1))	70.62(6)-71.92(8) (71.22(8))	69.98(7)-70.31(7) (70.17(7))

a) the averaged values are displayed in parentheses. *b*) ref. 2. *c*) ref. 3.

Table S3. Crystallographic Data and Details of the Refinement of **1c** and **2a**

	1c	**2a**
Formula	$C_{102}H_{138}Si_6P_6Pt_6 \cdot C_4H_8O$	$C_{66.5}H_{85}P_3Pt_3Si_4$, 2.5($C_4$)
formula wt	2961.12	1674.88
Temperature	90	90
cryst size/mm	0.034×0.047×0.076	0.026×0.046×0.048
cryst syst	monoclinic	triclinic
cryst color	yellow	red
space group	*P*2/c (*No*. 13)	*P*1 (*No*. 2)
a/Å	12.509(2)	12.607(2)
b/Å	18.884(3)	12.700(2)
c/Å	24.163(4)	23.579(5)
α/deg	90	77.301(3)
β/deg	90	84.488(3)
γ/deg	90	62.944(2)
V/Å^3	5707(2)	3280(1)
Z	2	2
D_{calcd}/g cm^{-3}	1.723	1.696
F(000)	2864	1638
μ/mm^{-1}	7.515	6.567
index ranges	$-16 \le h \le 16$ $-24 \le k \le 24$ $-19 \le l \le 31$	$-10 \le h \le 14$ $-14 \le k \le 14$ $-23 \le l \le 27$
no. of reflns meads	22755	15111
no. of unique reflns	9930	10622
R_{int}	0.0564	0.1379
no. of obsed reflns ($I > 2\sigma(I)$)	5668	5759
Restraints	732	900
Parameters	579	702
R, R_w ($I > 2\sigma(I)$)	0.0439, 0.0675	0.0610, 0.1331,
R, R_w (all data)	0.1026, 0.0780	0.1257, 0.1563
GOF on F^2	0.789	0.840

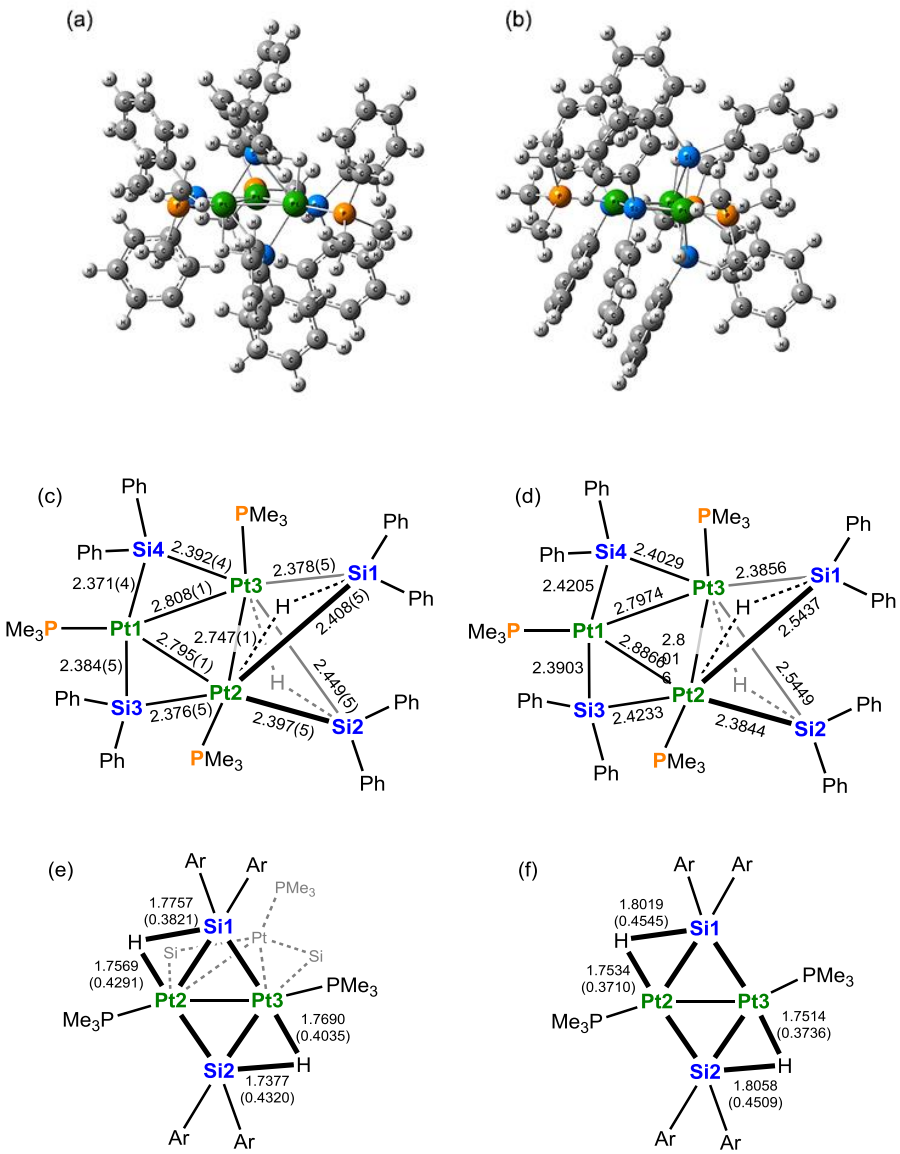

Selected Bond Distances (Å) and Wiberg Bond Index in Parenthesis

2.8016 (0.3723)	Pt2–Pt3	2.7431 (0.2980)
2.5438 (0.4428)	Pt2–Si1	2.4258 (0.4808)
2.3844 (0.6707)	Pt2–Si2	2.3674 (0.6570)
2.3857 (0.6726)	Pt3–Si1	2.3680 (0.6568)
2.5449 (0.4395)	Pt3–Si2	2.4275 (0.4812)

Figure S2. (a) Optimized structure and (b) its side view of **2a**. Selected bond distances of **2a** obtained from (c) X-ray results and (d) DFT calculations. Selected bond distances and Wiberg Bond Index around the bridging H ligand of (e) **2a** and (f) [{Pt(PMe_3)}$_2$(μ-η^2-$HSiPh_2$)$_2$] for comparison.

(a)

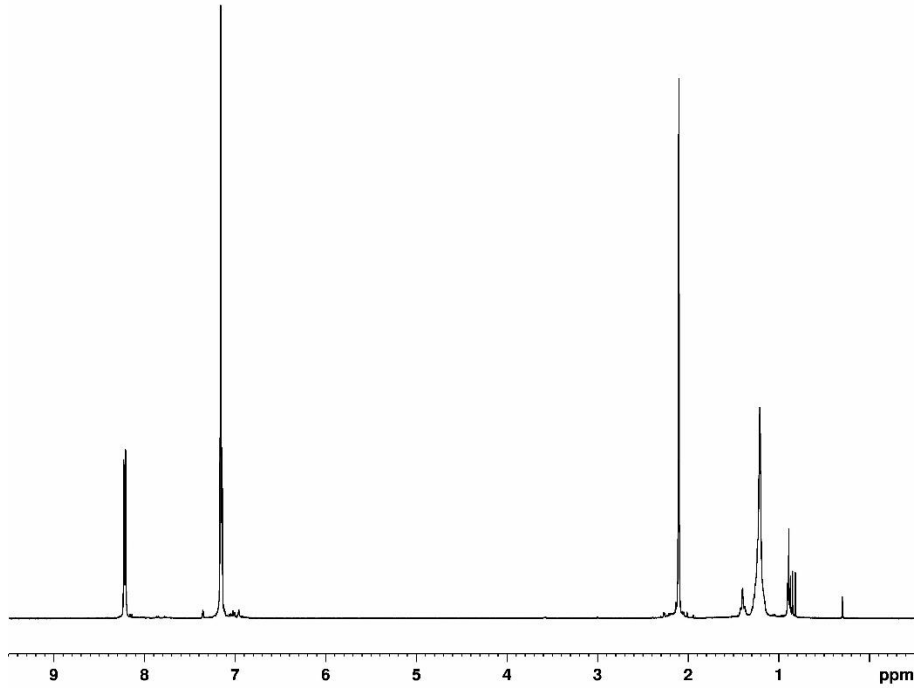

(b)

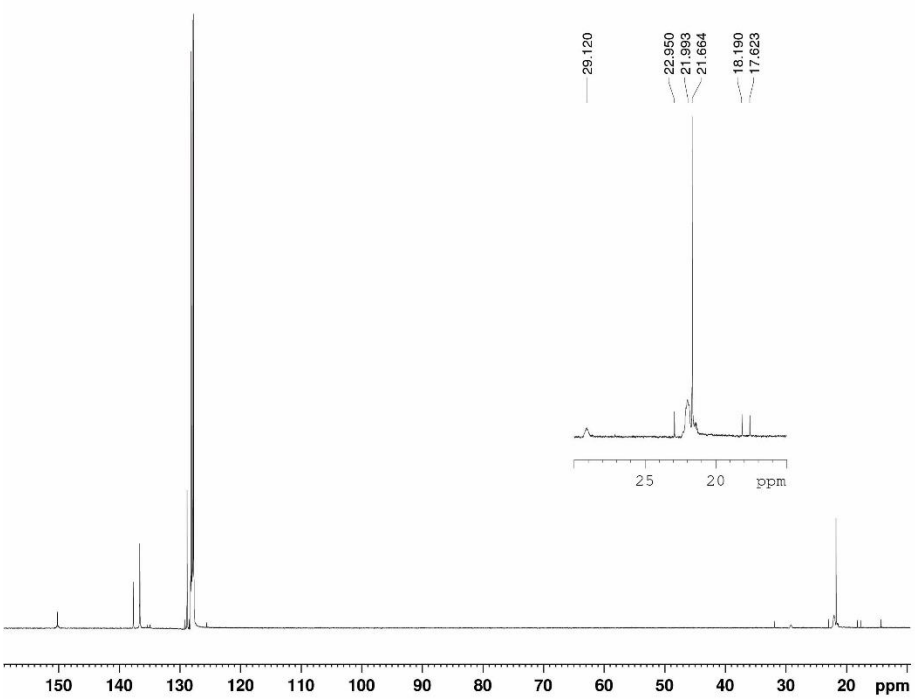

Figure S3. (a) ^{1}H NMR (400 MHz) and (b) ^{13}C{^{1}H} NMR (126 MHz) spectra of **1c** (C_6D_6, 298 K).

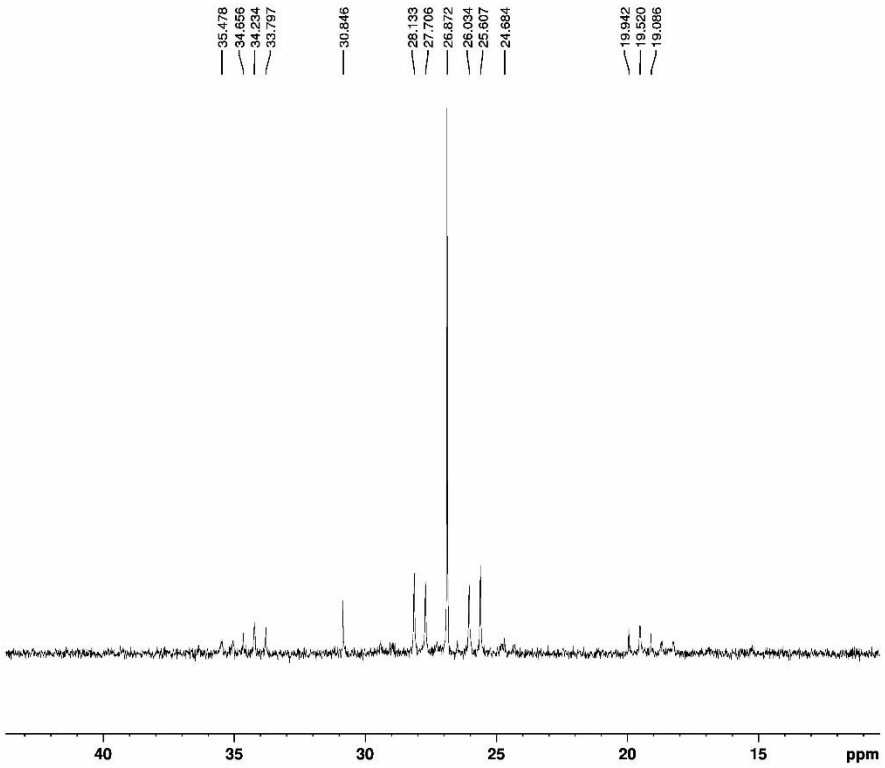

Figure S4. $^{31}P\{^{1}H\}$ NMR spectra of **1c** (202 MHz, C_6D_6, 298 K).

Table S4. The Coupling Constants [Hz] and Pt–Pt Bond Distances [Å] of Complexes **1a-c**

Ar	J_{PtP}	$^{2}J_{PtP}$	$^{3}J_{PP}$	J_{SiPt}	J_{PtPt}	Pt–Pt
1a[a] (Ar = C_6H_5)	2959	418	86	945	2950	2.697(1)-2.716(1)
1b[b] (Ar = C_6H_4-4-F)	2962	411	85	948	2500	2.7259(7)-2.7514(7)
1c (Ar = C_6H_4-4-Me)	2977	425	85	938		2.7018(8)-2.7093(5)

a) ref. 2. *b*) ref. 3.

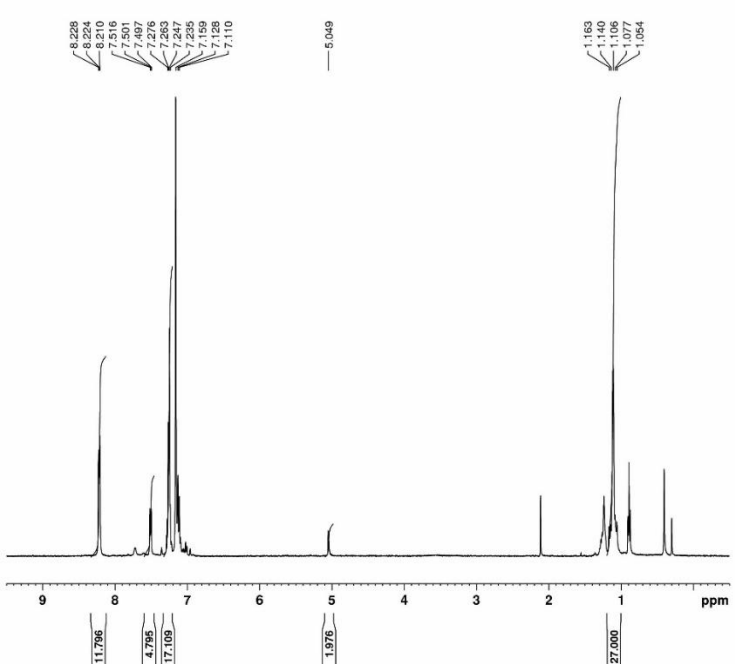

Figure S5. ^{1}H NMR spectrum after dissolution of isolated **2a**, giving **1a** and H_2SiPh_2 in 1:1 ratio (400 MHz, C_6D_6, r.t.).

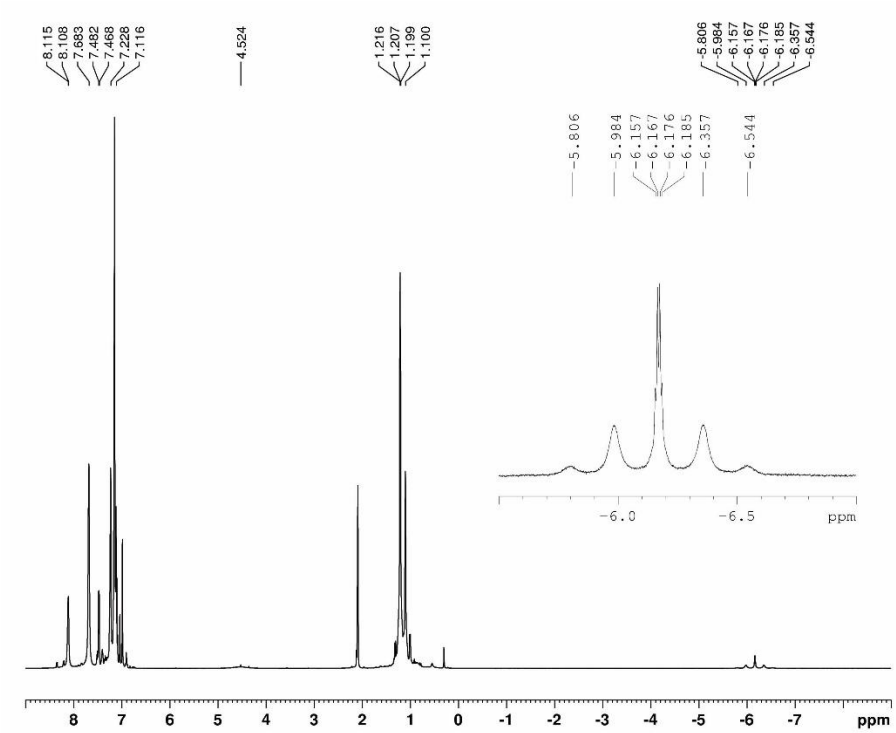

Figure S6. ^{1}H NMR spectrum of the mixture contains containing **2a** and H_2SiPh_2 in 1:3 ratio (500 MHz, toluene-d_8, 265 K).

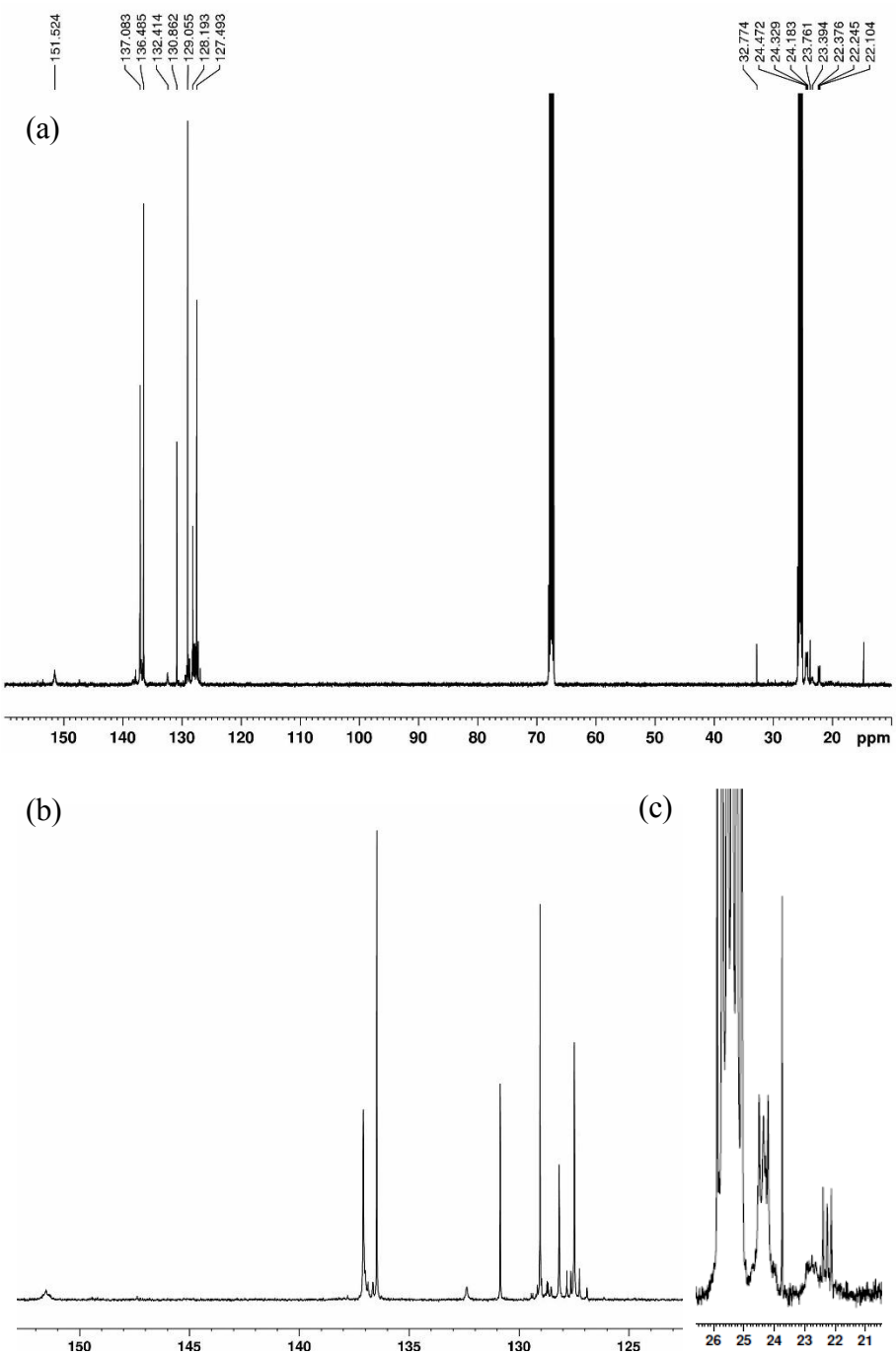

Figure S7. (a) $^{13}C\{^{1}H\}$ NMR spectra of the mixture contains containing **2a** and H_2SiPh_2 in 1:3 ratio (123 MHz, THF-d_8, 263 K), (b) in the aromatic region, and (c) in the PMe_3 region.

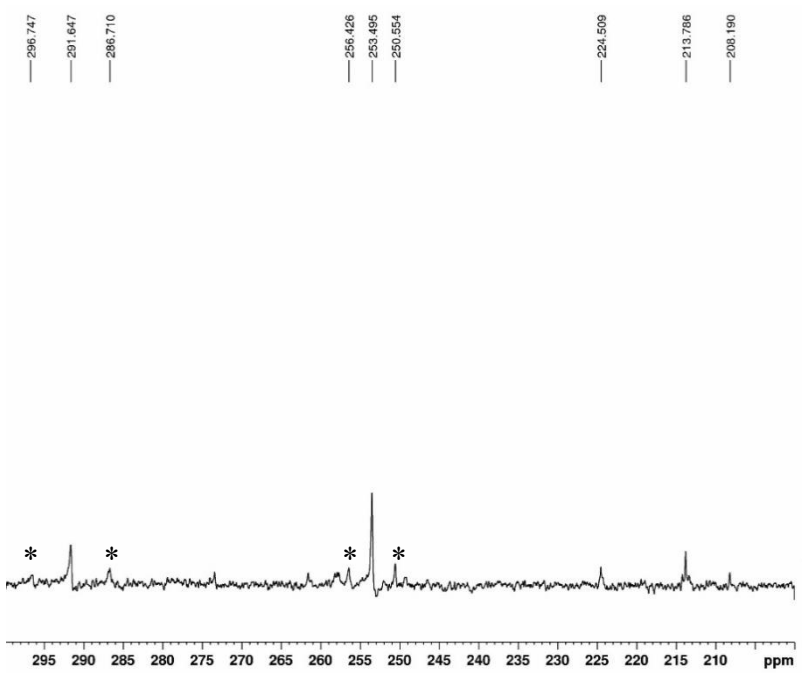

Figure S8. $^{29}Si\{^{1}H\}$ NMR spectrum of the mixture contains containing **2a** and H_2SiPh_2 in 1:3 ratio (99 MHz, THF-d_8, 263 K). The signals with asterisks are identified as satellite signals coupled with ^{195}Pt nucleus.

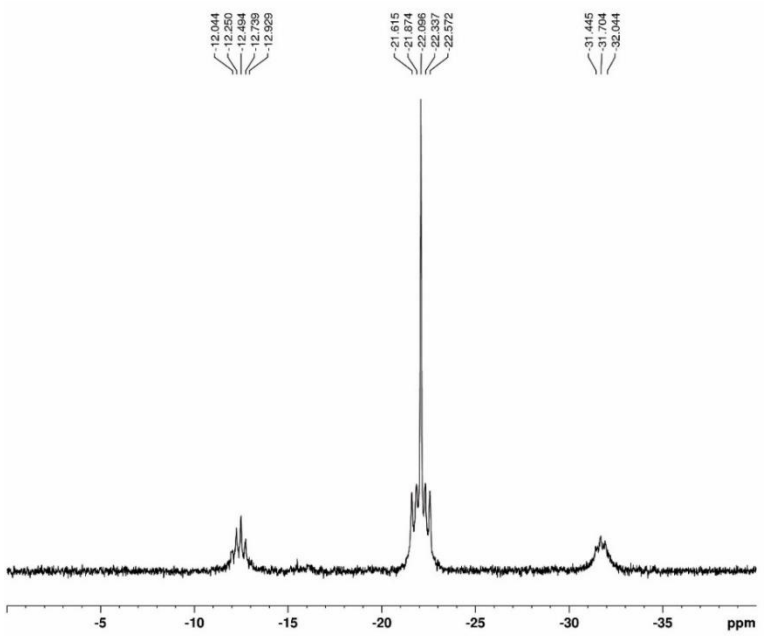

Figure S9. $^{31}P\{^{1}H\}$ NMR spectrum of the mixture contains containing **2a** and H_2SiPh_2 in 1:3 ratio (202 MHz, toluene-d_8, 265 K).

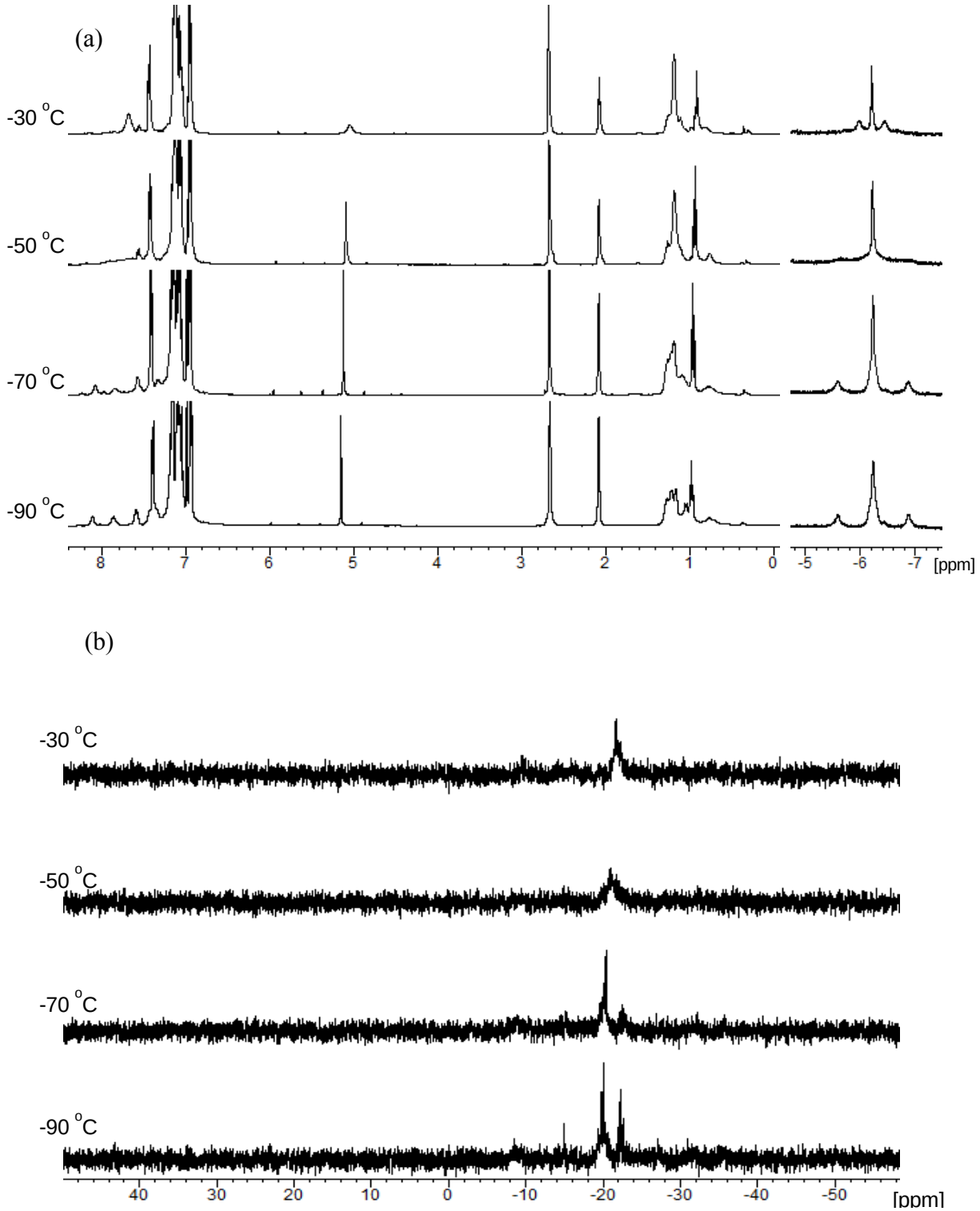

Figure S10. (a) ^{1}H NMR and (b) ^{31}P{^{1}H} NMR spectra of the mixture contains containing **2a** and H_2SiPh_2 in 1:3 ratio in toluene-d_8 at –30, –50, –70, and –90 °C.

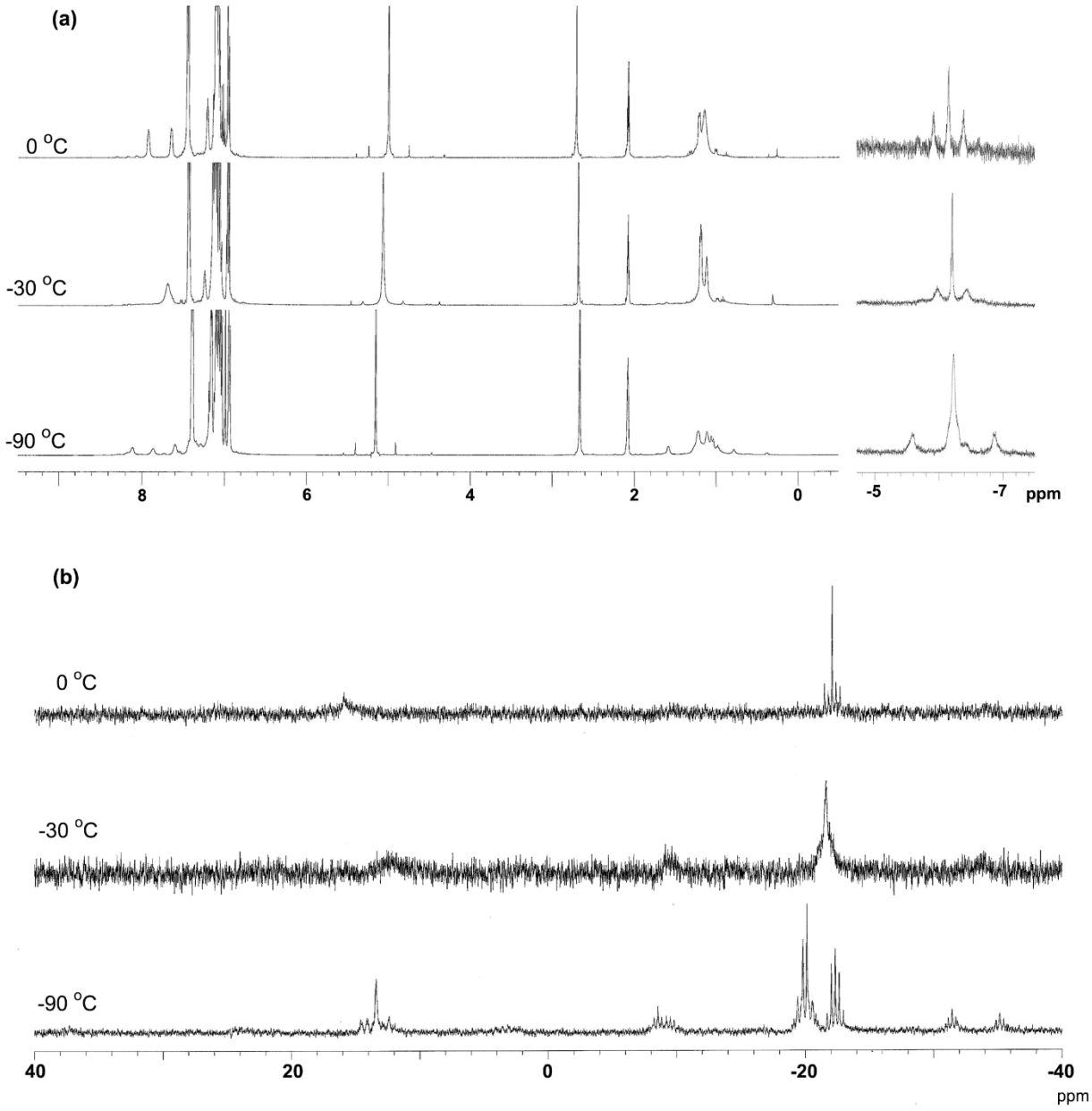

Figure S11. (a) ^{1}H NMR and (b) ^{31}P{^{1}H} NMR spectra of the mixture contains containing **2a** and H_2SiPh_2 in 1:10 ratio in toluene-d_8 at 0, –30, and –90 °C.

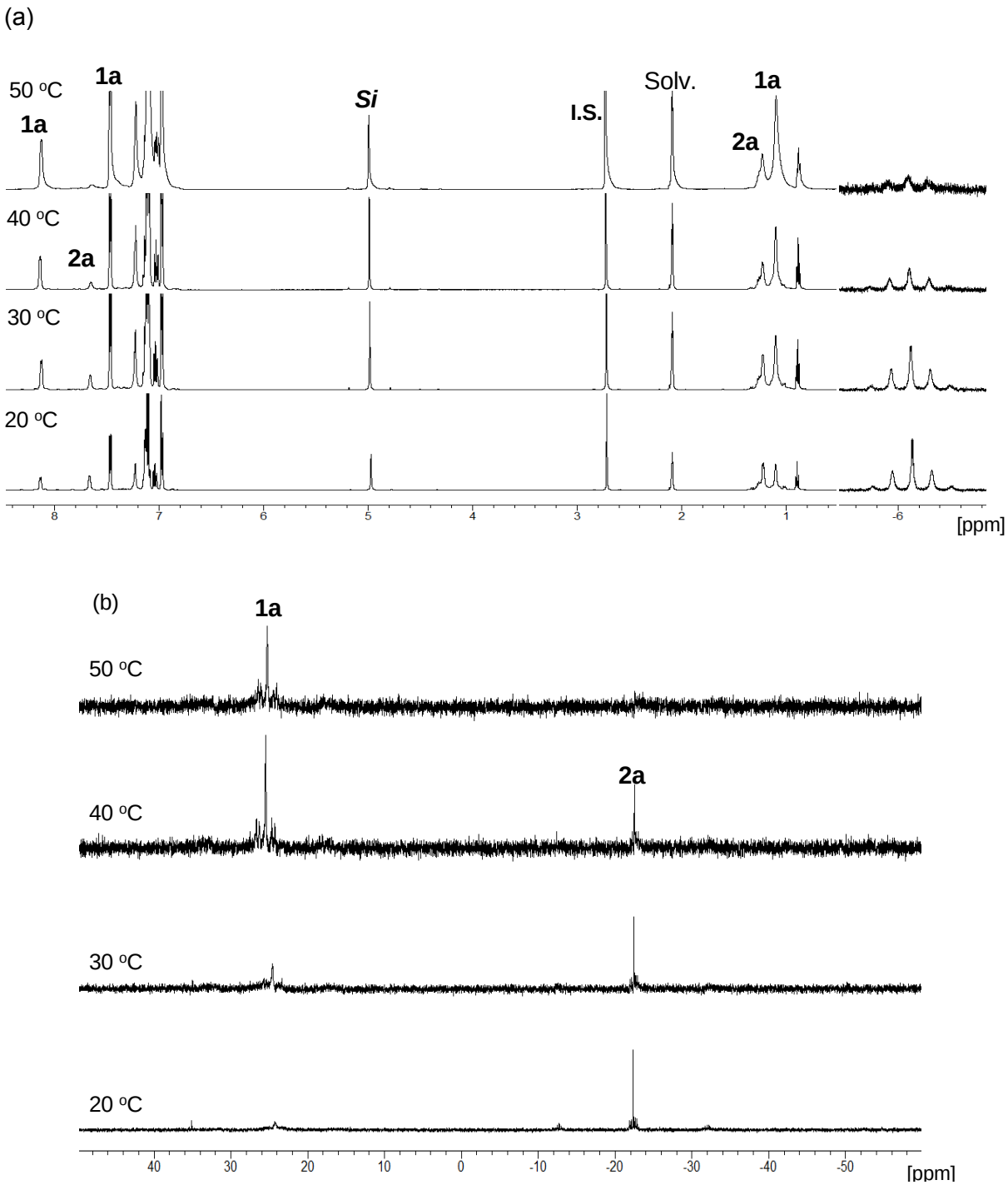

Figure S12. (a) ^{1}H NMR and (b) ^{31}P{^{1}H} NMR spectra of the mixture contains containing **2a** and H_2SiPh_2 in 1:3 ratio in toluene-d_8 at 20, 30, 40, and 50 °C. ***Si*** = H_2SiPh_2, **I.S.** = internal standard.

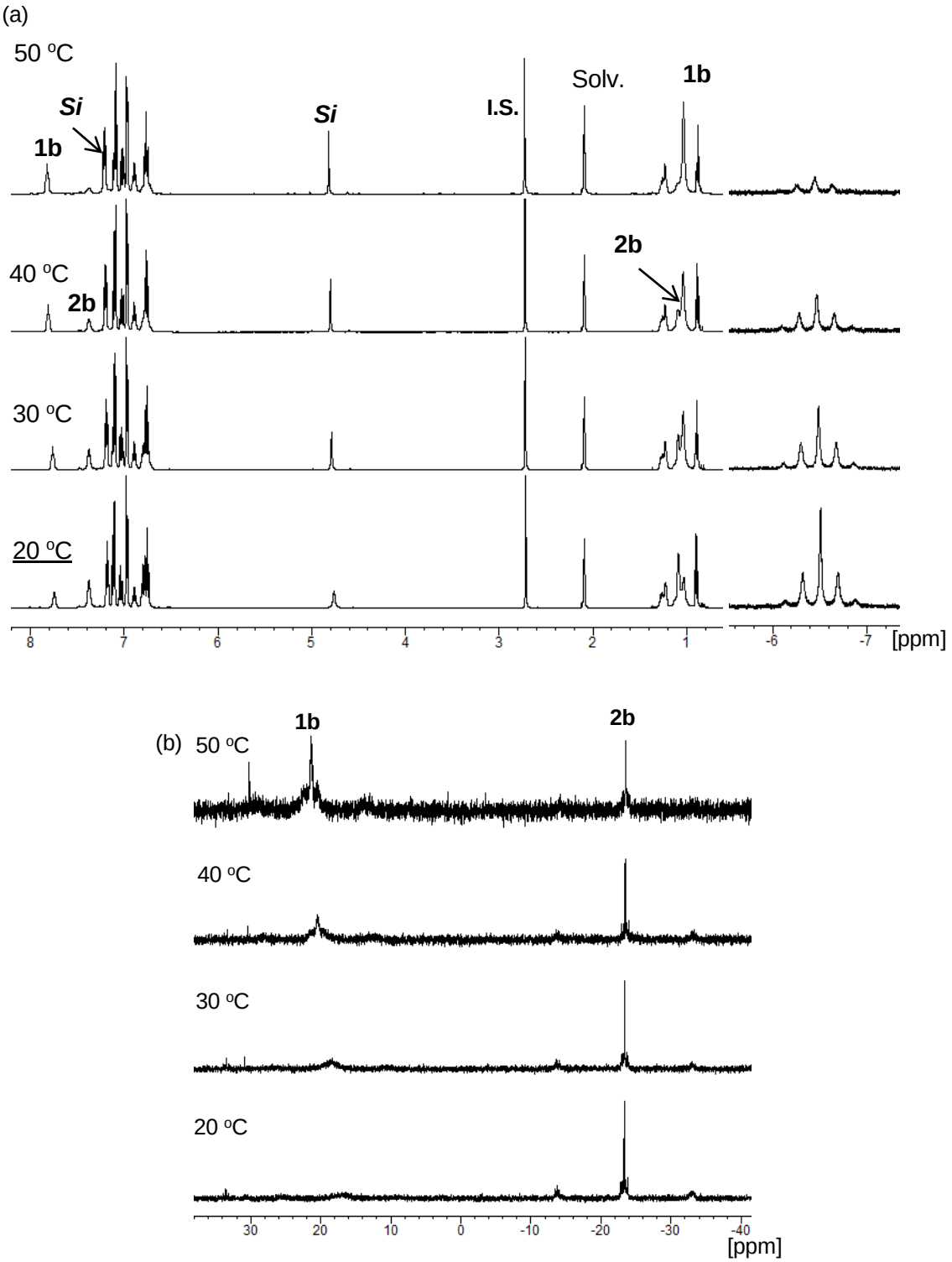

Figure S13. (a) ^{1}H NMR and (b) ^{31}P{^{1}H} NMR spectra of the mixture contains containing **2b** and $H_2Si(C_6H_4$-4-F) in 1:3 ratio in toluene-d_8 at 20, 30, 40, and 50 °C. ***Si*** = $H_2Si(C_6H_4$-4-F), **I.S.** = internal standard.

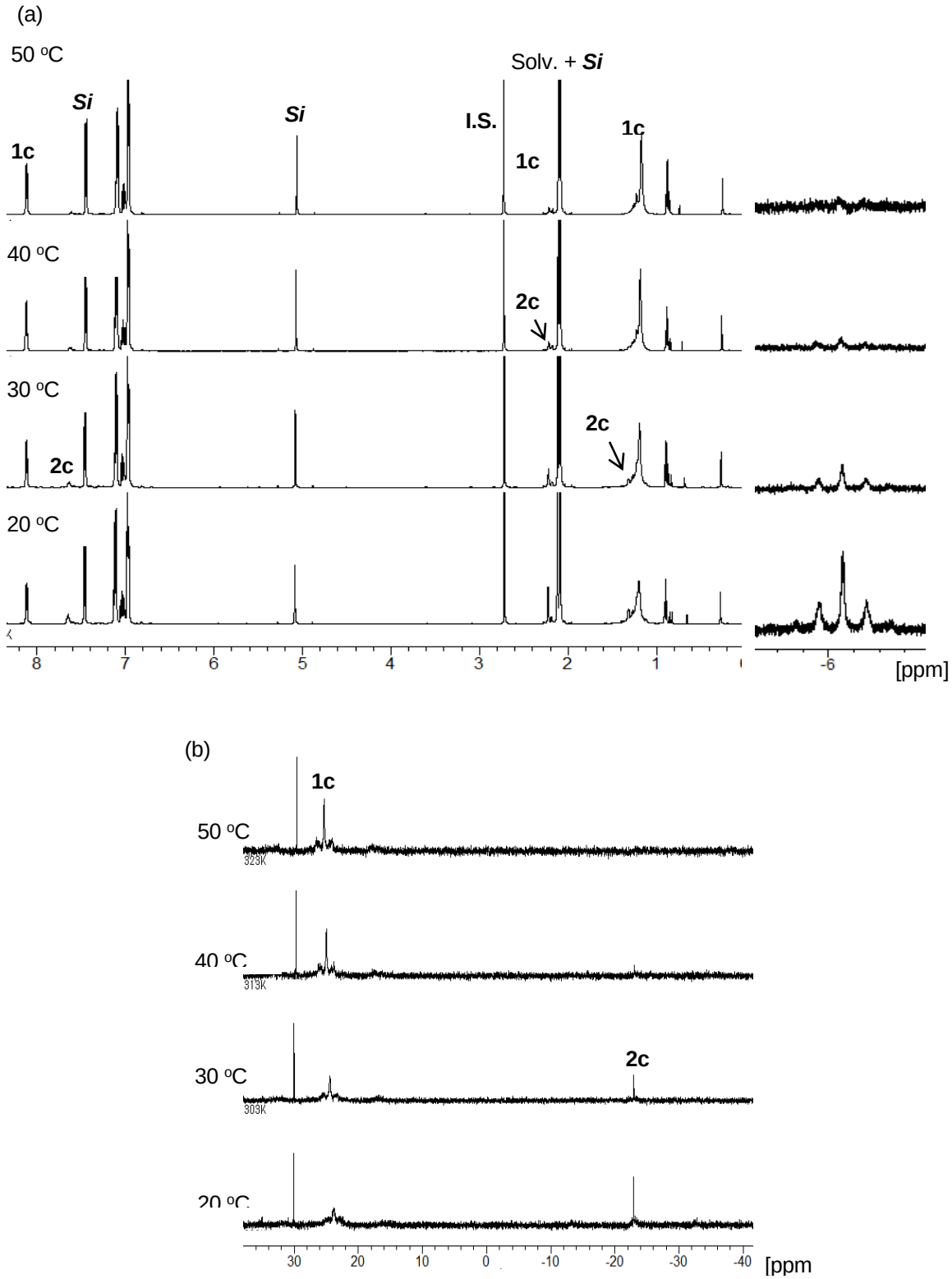

Figure S14. (a) ^{1}H NMR and (b) ^{31}P{^{1}H} NMR spectra of the mixture contains containing **2c** and $H_2Si(C_6H_4$-4-Me) in 1:3 ratio in toluene-d_8 at 20, 30, 40, and 50 °C. ***Si*** = $H_2Si(C_6H_4$-4-Me), **I.S.** = internal standard.

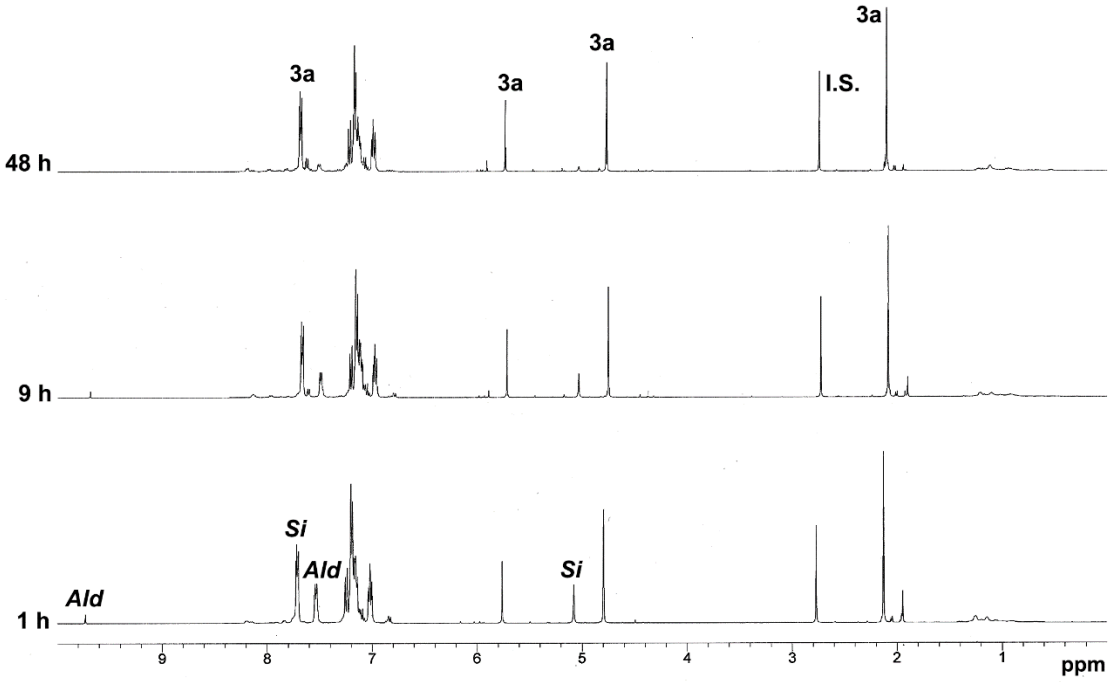

Figure S15. Monitoring ^{1}H NMR spectra of the mixtures in hydrosilyation of 4-methylbenzaldehyde with H_2SiPh_2 catalyzed by **1a** (400 MHz, C_6D_6, 298 K). ***Si*** = H_2SiPh_2, **I.S.** = internal standard.

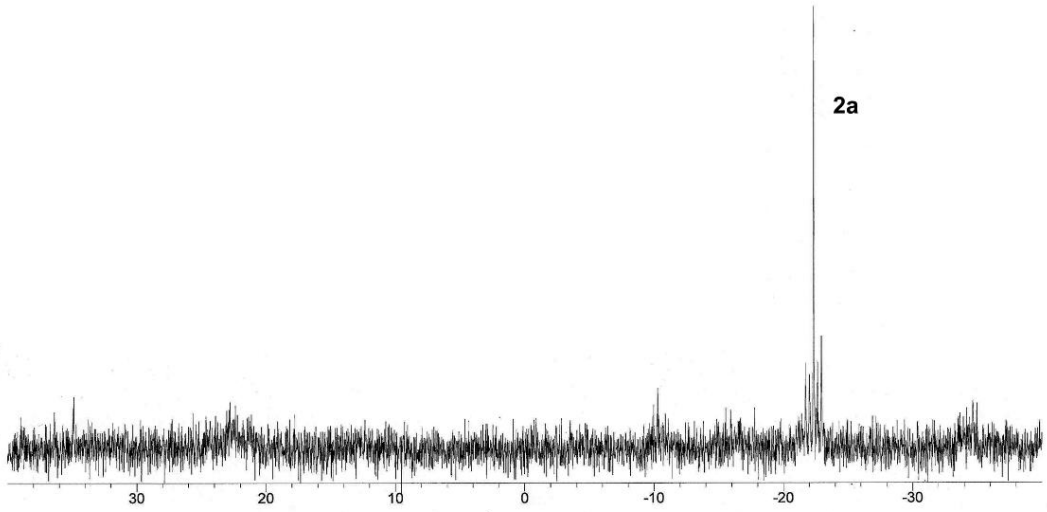

Figure S16. ^{31}P{^{1}H} NMR spectrum of the mixtures in hydrosilyation of 4-methylbenzaldehyde with H_2SiPh_2 catalyzed by **1a** after 1 h (400 MHz, C_6D_6, 298 K).

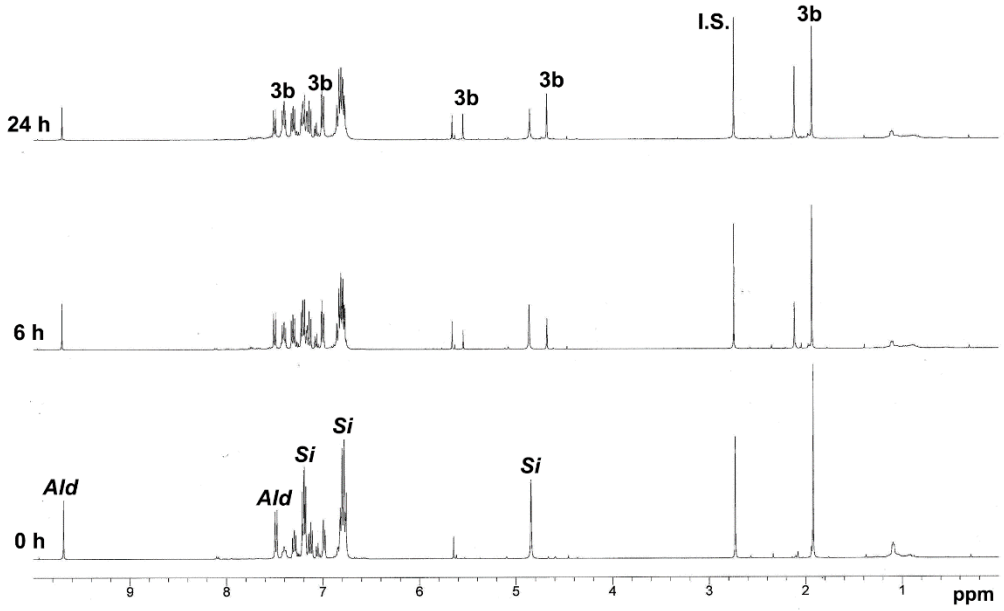

Figure S17. Monitoring ^{1}H NMR spectra of the mixtures in hydrosilyation of 4-methylbenzaldehyde with $H_2Si(C_6H_4\text{-}4\text{-}F)_2$ catalyzed by **1b** (400 MHz, C_6D_6, 298 K). ***Si*** = $H_2Si(C_6H_4\text{-}4\text{-}F)$, ***Ald*** = 4-methylbenzaldehyde, **I.S.** = internal standard.

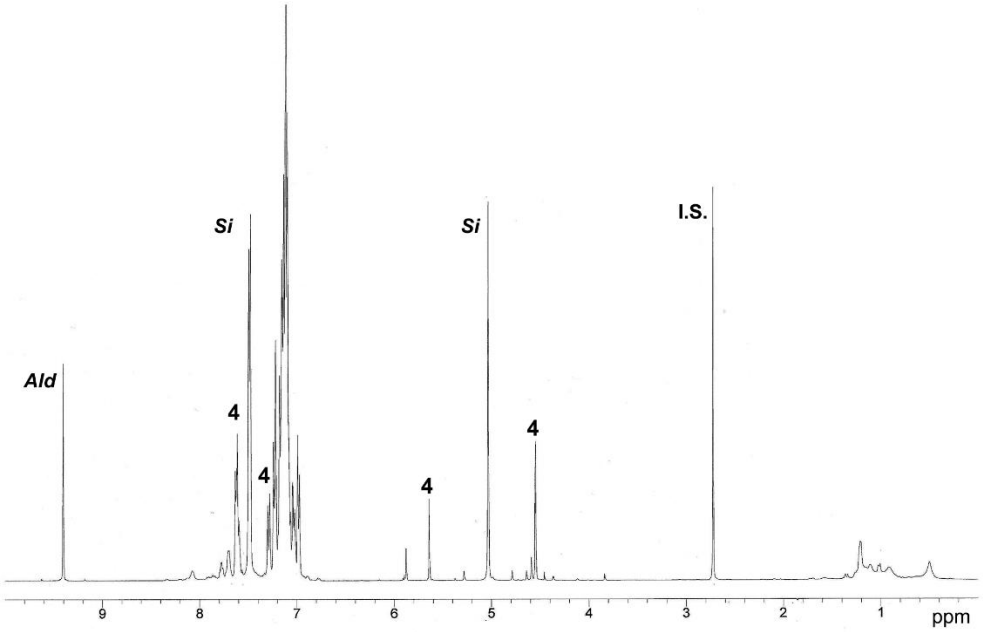

Figure S18. ^{1}H NMR spectrum of the mixtures in the hydrosilyation of 4-(trifluoromethyl)phenylaldehyde with H_2SiPh_2 catalyzed by **1a** (400 MHz, C_6D_6, 298 K). ***Si*** = H_2SiPh_2, **I.S.** = internal standard. ***Ald*** = 4-(trifluoromethyl)phenylaldehyde,

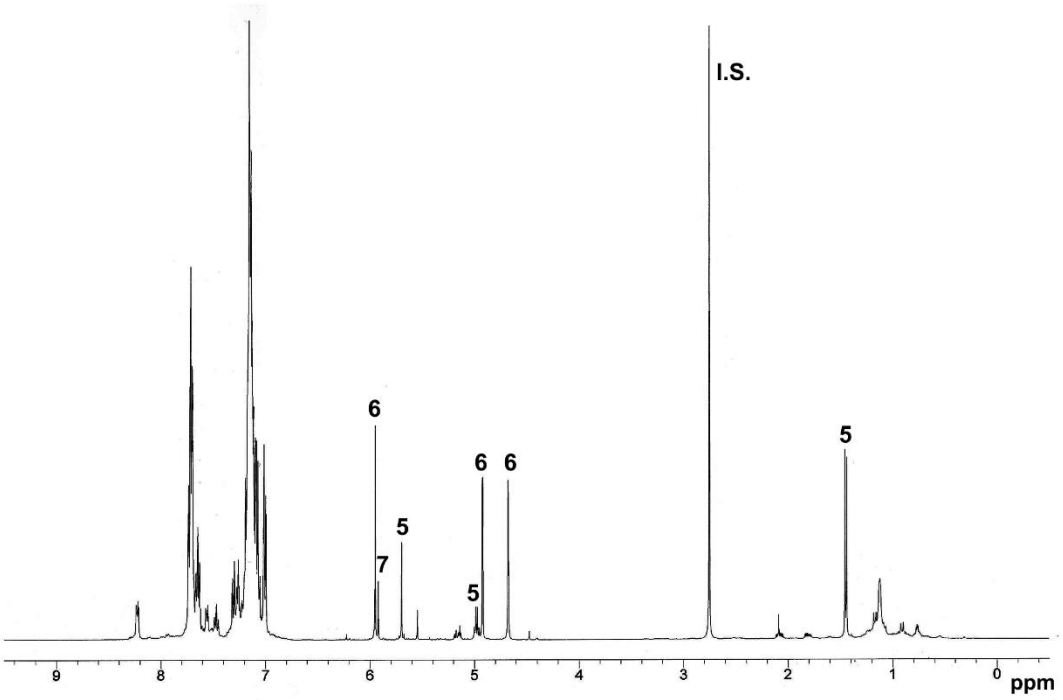

Figure S19. ^{1}H NMR spectrum of the mixtures in the hydrosilyation of methyl(phenyl)ketone with H_2SiPh_2 catalyzed by **1a** (400 MHz, C_6D_6, 298 K). **I.S.** = internal standard.

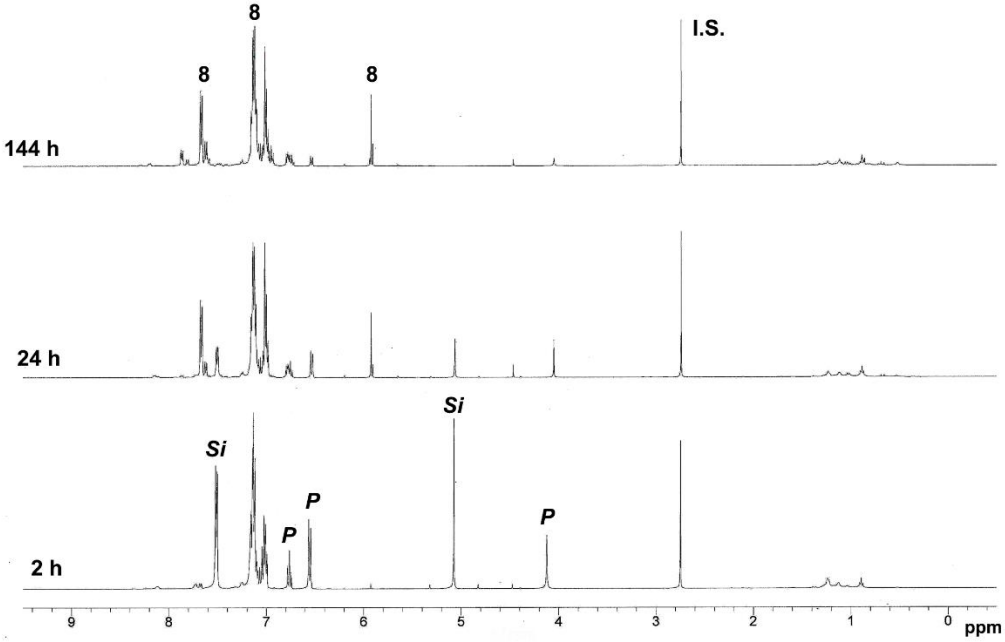

Figure S20. Monitoring ^{1}H NMR spectra of the mixtures in the dehydrocoupling of phenol and H_2SiPh_2 (400 MHz, C_6D_6, 298 K). ***Si*** = H_2SiPh_2, ***P*** = phenol, **I.S.** = internal standard.

References

1) Frisch, M. J.; Trucks, G. W.; Schlegel, H. B.; Scuseria, G. E.; Robb, M. A.; Cheeseman, J. R.; Scalmani, G.; Barone, V.; Mennucci, B.; Petersson, G. A.; Nakatsuji, H.; Caricato, M.; Li, X.; Hratchian, H. P.; Izmaylov, A. F.; Bloino, J.; Zheng, G.; Sonnenberg, J. L.; Hada, M.; Ehara, M.; Toyota, K.; Fukuda, R.; Hasegawa, J.; Ishida, M.; Nakajima, T.; Honda, Y.; Kitao, O.; Nakai, H.; Vreven, T.; Montgomery, Jr., J. A.; Peralta, J. E.; Ogliaro, F.; Bearpark, M.; Heyd, J. J.; Brothers, E.; Kudin, K. N.; Staroverov, V. N.; Kobayashi, R.; Normand, J.; Raghavachari, K.; Rendell, A.; Burant, J. C.; Iyengar, S. S.; Tomasi, J.; Cossi, M.; Rega, N.; Millam, N. J.; Klene, M.; Knox, J. E.; Cross, J. B.; Bakken, V.; Adamo, C.; Jaramillo, J.; Gomperts, R.; Stratmann, R. E.; Yazyev, O.; Austin, A. J.; Cammi, R.; Pomelli, C.; Ochterski, J. W.; Martin, R. L.; Morokuma, K.; Zakrzewski, V. G.; Voth, G. A.; Salvador, P.; Dannenberg, J. J.; Dapprich, S.; Daniels, A. D.; Farkas, Ö.; Foresman, J. B.; Ortiz, J. V.; Cioslowski, J.; Fox, D. J. Gaussian, Inc., Wallingford CT, 2009.
2) Osakada, K.; Tanabe, M.; Tanase, T. *Angew. Chem. Int. Ed*. **2000**, *39*, 4053–4055.
3) Tanaka, K.; Kamono, M.; Tanabe, M.; Osakada, K. *Organometallics* **2015**, *34*, 2985–2990.